PCCP

Accepted Manuscript

ROYAL SOCIETY OF CHEMISTRY

www.rsc.org/pccp

Journal Name

ARTICLE TYPE

Cite this: DOI: 10.1039/xxxxxxxxxx

How do non-Covalent Complexes Dissociate in Droplets? A case study of the Desolvation of dsDNA from a Charged Aqueous Nanodrop†

Mahmoud Sharawy,*[a] and Styliani Consta,[a‡]

Received Date
Accepted Date

DOI: 10.1039/xxxxxxxxxx

www.rsc.org/journalname

We present the desolvation mechanism of a double-stranded oligodeoxynucleotide (dsDNA) from an aqueous nanodrop studied by using atomistic molecular dynamics methods. Central theme in this study is the stability of a non-covalently bound complex, in general, and that of a dsDNA in particular, in the droplet environment. Among the factors that may affect the stability of a complex in an evaporating droplet we examine the increase in ion concentration and the distinct droplet morphologies arising from the charge-induced instability. We explore in detail a large set of aqueous nanodrops with excess negative charge, which comprise a dsDNA and Na^+, Cl^- ions at various concentrations. We find that for a square of the charge to volume ratio above that of the Rayleigh limit the droplet attains distinct "spiky" morphologies that disperse the charge in larger volume relative to that of the spherical drop. Moreover, it is found that it is possible for a non-covalent complex to remain associated in an unstable droplet as long as there is enough solvent to accommodate the instability. In the presence of Na^+ and Cl^- ions, the Na^+ ions form adducts with the double helical DNA in the minor groove, which help stabilise the duplex state in the gas phase. The negative ions may be released from the droplet. In a DNA-containing droplet with a net charge that is less negative than 50% of the dsDNA charge, the DNA maintains a double-stranded state in the gas phase. Several of our findings are in good agreement with experiments, while the spiky droplet morphology due to the charge-induced instability calls for new experiments. The results shed light on the association properties of complexes of macromolecules in droplet environments, which are critical intermediates in electrospray ionisation experiments.

1 Introduction

Detection of the non-covalent interactions within a protein-ligand, a protein-nucleic acid and a nucleic acid complex has attracted considerable attention over the past twenty years.[1–4] Study of the association properties of biological macromolecules is important for the understanding of cell functions. Moreover, association properties play an important role in the analyses of protein and nucleic acid complexes in analytical chemistry. A broadly used experimental technique to study these interactions is electrospray ionization mass spectrometry (ESI-MS)[4–13]. Electrospray ionization transfers macromolecules from a bulk solution into the gas phase via the generation of droplets. In nano-ESI the solution is dispersed into a fine aerosol of nanodrops, which have initially a radius of approximately 150 nm and contain excess of thousands of elementary charges.[14] In these droplets the solvent is often water and the ions are ammonium, acetate and impurities such as sodium and chloride.[15] Once the nanodrops had been generated they decrease in size by the emission of excess charged species and by solvent evaporation. This constantly evolving droplet environment is different from that of the mother bulk solution or that of a neutral droplet with a low concentration of ions. The reason for the difference is that an electrosprayed droplet is characterised by: high concentration of ions relative to that of the bulk solution; strong electric field due to the presence of charged macromolecules or complexes; large surface to volume ratio, which is, in general, the main difference between bulk and finite sized systems[16–21]. This new environment may affect the association properties within a non-covalent complex differently from the bulk solution. Unfortunately, the effect of the evaporating droplet on the non-covalent interactions cannot be readily detected in experiments. Because of the still unresolved droplet effects, the preservation of the complex interactions in its journey from the bulk solution to the gas phase has been hotly debated

[a] Department of Chemistry, The University of Western Ontario, London, Ontario, Canada N6A 5B7.

‡ Present Address: Department of Chemistry, University of Cambridge, Lensfield Road, Cambridge, CB2 1EW, United Kingdom. E-mail: sc904@cam.ac.uk

† Electronic Supplementary Information (ESI) available: Movies S1–S3 and Figures S1, S2, S3. See DOI: 10.1039/b000000x/

among the scientists who use ESI.[5,6,8]

It has been recognised that there are two major factors that affect the association of units in a complex: the evaporation rate and the finite size of the droplet.[1,22] The latter one infers that the two species can be brought together even though they may be separated in the bulk solution. These two effects have been identified indirectly by experimental investigation. Effects that have not been considered so far are the increase in the concentration of ions in evaporating droplets and the distinct droplet morphologies arising from the charge-induced instability. These are the two effects that are examined in the present study.

We examine the stability of a double-stranded DNA duplex (dsDNA) in an evaporating aqueous droplet by using atomistic molecular dynamics simulations. The dsDNA is used as a paradigm of a complex of macromolecules to helps us understand the principles of desolvation that hold for a large number of complexes and macromolecules. The dsDNA was used in our study for the following reasons. The dsDNA is a naturally charged complex of macromolecules with charge $-2\,e$ (where e denotes the elementary positive charge) per base pair, therefore, the charge distribution is well defined along the macromolecules in moderate to high pH. The dsDNA complex is relative stiff; therefore, the problem of sampling the conformations is less severe than that for flexible macromolecules such as poly(ethylene glycol)[23]. The third reason is the significant practical applications of DNA in general. It is well known that DNA plays a critical role in biology and medicinal research. Synthetic oligodeoxynucleotides have been used as gene probes, in complementary DNA hybridisation experiments and in gene therapy.[24–27] As with any other biological molecule, it is important to characterise synthetic oligodeoxynucleotides upon their preparation. ESI-MS is one of the most commonly used method to characterise oligodeoxynucleotides.

Light-Wahl et al.[28], who first observed the dsDNA complex by ESI-MS, have already posed the fundamental questions regarding the origin of the signals in the mass spectrum. In their experiments mild electrospraying and desolvation conditions led to the observation of the dsDNA signal. At the same time, signals of the monomeric constituents were also identified. In ESI-MS experiments it has also been found that the intact duplex was not observed when dsDNA was sprayed from distilled deionized water. The natural questions that arise are how the desolvation process affects the stability of the dsDNA and how the ions affect the duplex stability.

Molecular simulations may provide insight into the stability of dsDNA in droplets. We found that, so far, the number of computational studies is very limited. The computational studies of dsDNA dynamics and interactions have been restricted to either one of the two cases, bulk solvent[29–31] or gas phase.[32] Many of previous studies on dsDNA have not adequately addressed the following questions: the morphologies of a charged nanodrop containing DNA, the complete process of solvent and ion evaporation, a complete description of the charge states of dsDNA in the gas phase, and the minimum concentration of cations required to stabilise the duplex state of dsDNA in the gas phase.

To answer these questions we perform atomistic molecular dynamic simulations of the 11-mer all adenine-thymine (A·T) DNA duplex in aqueous nanodrops with various concentrations of sodium and chloride ions. We examine two settings of aqueous droplets that contain a $[\mathrm{dsDNA}]^{20-}$. In the first setting the droplet is composed of water and a sole $[\mathrm{dsDNA}]^{20-}$, which renders the droplet its negative charge. In the other setting the aqueous droplet contains $[\mathrm{dsDNA}]^{20-}$ and ions (Na^+ and Cl^-). The principles of the desolvation found in our studies are not restricted to the particular $[\mathrm{dsDNA}]^{20-}$ complex. Nucleic acids but also peptides[33] may show similar desolvation behavior, which enables us to find universal patterns of desolvation.

Theoretically, the emission of single charged species has been explained by Rayleigh's model[21,34] and ion-evaporation mechanism.[35,36] In Rayleigh's model the stability of a droplet is determined by two competing factors: the surface tension force that holds the droplet intact and the Coulomb repulsion between the charges of the same sign that tends to fragment the droplet. The Rayleigh's model dictates that the stability of the droplet with respect to small fluctuations is determined by the ratio the square of the charge to the droplet volume. The critical value of this ratio where the two competing factors compensate each other is known as the Rayleigh limit, which reads:

$$Q^2 = 64\pi^2\varepsilon_0\gamma R_0^3 \qquad (1)$$

where Q denotes the charge of the droplet, ε_0 the vacuum permittivity coefficient, γ the surface tension and R_0 the radius of the droplet. When the surface interactions are dominant (the droplet is said to be found below the Rayleigh limit), the droplet evolves through evaporation of solvent molecules until it reaches the Rayleigh limit. At that moment the charged species are released to remove the excess charge. The droplet is found once more below the Rayleigh limit. This cascade of evaporation and fission events continues till the droplet disintegrates completely. We want to emphasise at this point that Rayleigh's model deals with mobile charges. When the charge is bound on a macromolecule or in complexes of macromolecules the validity of Rayleigh's model becomes questionable. Simulations have revealed that a charged macromolecule[33] or complexes of macromolecules[19] may induce instabilities that cannot be described by the conventional description of the surface energy as the product of surface tension times surface area. These simulation findings have been discussed in Ref. [19,33]. In the present study we examine the various manners that the charge-induced instability of the droplets is manifested during desolvation. In the analysis of the data we compare the simulation findings with Rayleigh's model and we address its validity.

2 Model and computational methods

To study the stability of a dsDNA in aqueous droplets, we simulated droplets that were composed of (i) water and a sole $[\mathrm{dsDNA}]^{20-}$ and (ii) water, $[\mathrm{dsDNA}]^{20-}$, Na^+ and Cl^- ions. The $[\mathrm{dsDNA}]^{20-}$ that we used in this study was the 11-mer A·T dsDNA ($\mathrm{d(ApApApApApApApApApApA)_2}$). The 5′ ends lack a phosphodiester linkage at the 5′ positions and are terminated by a hydroxyl group. The 20 phosphodiester linkages were fully deprotonated and gave a total charge of $-20\,e$. The helical structure was initially in B-tract conformation and made one turn. The $[\mathrm{dsDNA}]^{20-}$ was solvated by water molecules modelled by

the transferable intermolecular potential function (TIP3P) [37] with flexible bonds and angle bending. Hereafter, we use the O1P and O2P notations to denote the two oxygen atoms of the phosphodiester linkages. A typical snapshot of the system is shown in Fig. 1.

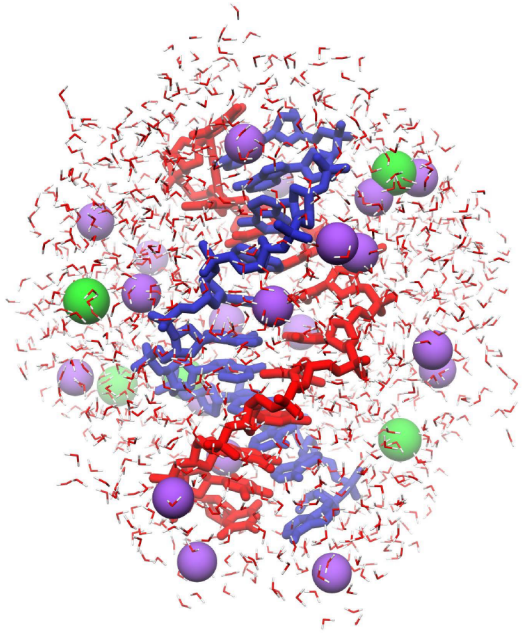

Fig. 1 Representation of a typical water droplet composed of the 11-mer A·T dsDNA and ions. The ribbons represent the backbone of DNA. The sizes of the water molecules, Na^+ (purple), and Cl^- (green) ions are rescaled for clarity.

We used the GROMACS [38] version 4.6.5 computational package for the molecular simulations and Visual Molecular Dynamics (VMD) [39] for the visualisations of the simulations. The dsDNA complexes were modelled using the AMBER99SB-ILDN [40] force field where all hydrogen atoms are explicitly represented. This force field includes optimised potential terms for bond-stretching and angle bending vibrations, which are described by an ideal harmonic oscillator, as well as torsional strains, Coulombic electrostatic interactions, and Lennard-Jones (LJ) interactions. The cross interactions between two sites i and j are estimated by the combining rules $\varepsilon_{ij} = (\varepsilon_i \varepsilon_j)^{1/2}$ and $\sigma_{ij} = (\sigma_i \sigma_j)^{1/2}$, where ε_i and σ_i denote the depth of the LJ potential and the diameter of the atomic species i, respectively. To create a series of systems with various net charges and ion composition, we solvated the dsDNA in TIP3P water and then added the Na^+ and Cl^- ions at random positions in the droplet. For every concentration of ions we created a set of two initial conditions. The initial compositions of the duplicates are presented in Table 1.

Simulations were performed using the molecular dynamics (MD) Velocity Verlet algorithm. The droplets were modelled in vacuo and in the treatment of the electrostatic interactions no cut-off was used. The simulations were carried out in series of 0.5 ns constant temperature runs. Because the evaporated ions and water molecules that are far from the dsDNA have weak interactions with it, the evaporated water molecules and ions were removed every 0.5 ns when they were located outside a radius of 70 nm from the dsDNA. The time step used in all the simulations was 0.5 fs, that is 13 times smaller than the fastest O-H vibration in the system. The simulations were terminated when the dsDNA was in gas phase or when the two strands were separated. In the most of the realisations the total time length of the runs ranged between 5 ns to 42 ns.

Table 1 Initial composition of aqueous droplets containing $[\mathrm{dsDNA}]^{20-}$. The droplets composed of 6500 H_2O were simulated with and without temperature control to test the outcome of the the Nosé-Hoover algorithm.

System	Net Charge/e	H_2O	Conc./mM	
			Na^+	Cl^-
$[\mathrm{dsDNA}]^{20-}$	−20	6500	0	0
$[\mathrm{dsDNA}]^{20-} + 10\,Na^+$	−10	6500	77	0
$[\mathrm{dsDNA}]^{20-}$	−20	1500	0	0
$[\mathrm{dsDNA}]^{20-} + 5\,Na^+ + 5\,Cl^-$	−20	1500	141	141
$[\mathrm{dsDNA}]^{20-} + 10\,Na^+ + 10\,Cl^-$	−20	1500	281	281
$[\mathrm{dsDNA}]^{20-} + 5\,Na^+$	−15	1500	141	0
$[\mathrm{dsDNA}]^{20-} + 10\,Na^+ + 5\,Cl^-$	−15	1500	281	141
$[\mathrm{dsDNA}]^{20-} + 15\,Na^+ + 10\,Cl^-$	−15	1500	422	281
$[\mathrm{dsDNA}]^{20-} + 10\,Na^+$	−10	1500	281	0
$[\mathrm{dsDNA}]^{20-} + 15\,Na^+ + 5\,Cl^-$	−10	1500	422	141
$[\mathrm{dsDNA}]^{20-} + 20\,Na^+ + 10\,Cl^-$	−10	1500	563	281
$[\mathrm{dsDNA}]^{20-} + 15\,Na^+$	−5	1500	422	0
$[\mathrm{dsDNA}]^{20-} + 20\,Na^+ + 5\,Cl^-$	−5	1500	563	141
$[\mathrm{dsDNA}]^{20-} + 25\,Na^+ + 10\,Cl^-$	−5	1500	704	281

To maintain constant temperature, the systems were thermalised using the Nosé-Hoover thermostat. A transient time period of 2 ns was sufficient to allow for a droplet to reach a natural configuration and a mixed distribution of the ions in the droplet. The effect of the Nosé-Hoover algorithm on the simulation findings was tested on the two large nanodrops composed of 6500 water molecules (Table 1). In these tests, we thermalised one from each system duplicate at $T = 350$ K for 2 ns, decoupled it from the thermostat and then we continued the simulation without a temperature control. The dynamics was compared with the second duplicate that was simulated at constant temperature until the dsDNA was in the gas phase. An expected difference in the dynamics between the systems with and without temperature control was the cooling of the droplets without the thermostat. This had no profound effect on the results we report here regarding the manners that the charge-induced instabilities are manifested and the role of the ions in the stability of the dsDNA. Additional information on the parameters of the simulations is found in the Electronic Supporting Information Figures S1 and S2. In this study, we report the results of the constant temperature simulations at $T = 350$ K.

3 Results and Discussion

3.1 Desolvation of $[\mathrm{dsDNA}]^{20-}$ from a charged aqueous nanodrop

At first we study the desolvation of a dsDNA with charge $-20\,e$ from an aqueous droplet. Fig. 2 shows typical snapshots of the dsDNA desolvation starting from a droplet of 6500 H_2O molecules (which has radius ≈ 4.0 nm). The initial state of the nanodrop (Fig. 2-i) shows a clear stability demonstrated by its spherical shape. Rayleigh's critical charge for this droplet size is $-22\,e$, therefore the nanodrop is found below the Rayleigh limit. This critical charge was estimated by Eq. 1 where the surface tension of value 0.0432 N/m at $T = 350$ K for TIP3P water model [41] was used as in our previous studies [42]. As the nanodrop volume decreases, because of water evaporation, the nanodrop enters the charge-induced instability regime (Fig. 2-ii–v). In this regime, the droplet shape deforms. The deformation starts when the droplet has approximately 4820 H_2O molecules. In this number we may add other 310 H_2O molecules to account for the size of the dsDNA that it is included in the droplet. Therefore, simulations indicate that a droplet with charge $-20\,e$ will deform at 5130 H_2O molecules vs. 5940 predicted by Rayleigh. A small change in the surface tension from 0.0432 N/m to 0.05 N/m may account for this difference in the number of molecules. Given the simplicity of Rayleigh's model, its prediction is close to the simulation findings. We note here, that differently from the case of separated charged species in a droplet, the dsDNA is not mobile, therefore, Rayleigh's assumption for a conductive droplet is no longer valid. This break-down may be another reason for the small

discrepancy between the theoretically predicted and simulation value.

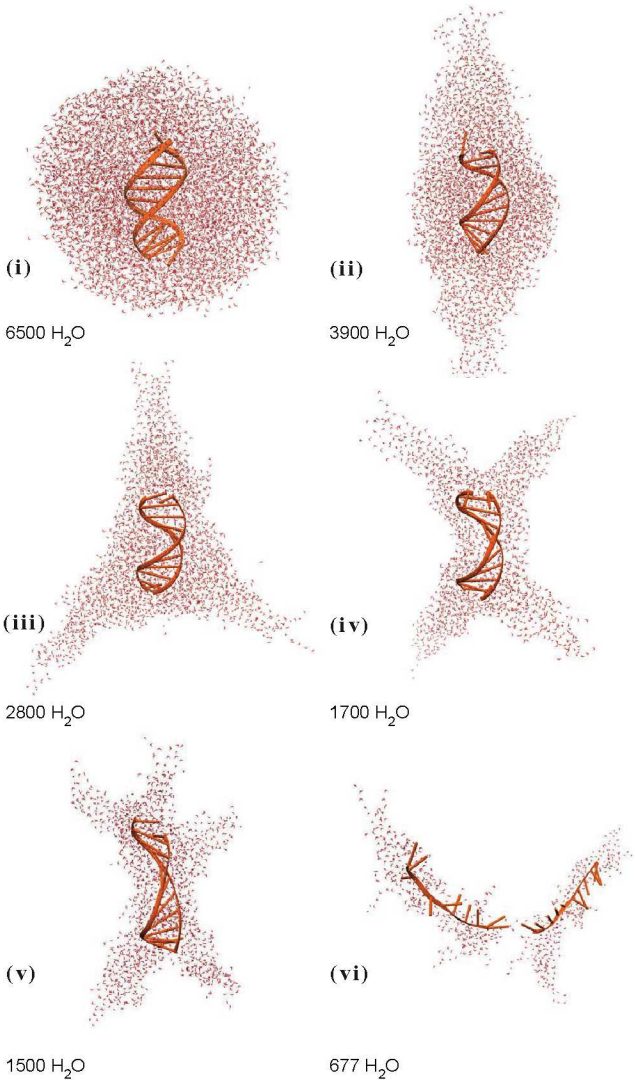

Fig. 2 Desolvation of a droplet composed of 6500 H_2O and dsDNA. The overall charge of the droplet is $-20\,e$ and it is carried by the dsDNA. This charge remains constant throughout the desolvation. The droplet size during the droplet evolution is indicated in every panel. At $T = 350$ K (constant temperature runs) the approximate relative times (by setting the time origin to zero in the snapshot (i)) that the instabilities appear are (i) $t = 0$; (ii) 6.2 ns; (iii) 9.1 ns; (iv) 12.5 ns, (v) 13.1 and (vi) 17.5 ns.

Here we comment on typical stages of the desolvation process where the droplet morphologies change dramatically. For instance, when the droplet contains 3900 H_2O molecules (Fig. 2-ii) the Rayleigh critical charge is $-19\,e$; therefore, the nanodrop is above the Rayleigh limit. Since the charge carriers are covalently bonded within the dsDNA, the charge-induced instability cannot be manifested by droplet fragmentation.[16,17,20] Instead, the nanodrop deforms by forming two conical ends at the termini of the duplex (Fig. 2-ii). The tips of the conical ends are 15.5 nm apart and the radius of the middle region is approximately 2.3 nm. The dsDNA still maintains its initial length (≈ 3.7 nm). Further evaporation of water increases the instability of the nanodrop and results in the division of one of the conical ends into two "spikes" (Fig. 2-iii). At a later stage, evaporation leads to the appearance of a fourth spike stemming from the division of the conical end at the other pole (Fig. 2-iv). As two spikes are formed on either ends of the duplex, they are located on opposite sides a plane that passes through the helix axis forming a staggered arrangement. This staggered conformation counteracts the electrostatic steric interactions between the two spikes. The number of spikes increase gradually (Fig. 2-i–v), as the volume of the nanodrop decreases by the water evaporation. In the final stage (Fig. 2-v) the dsDNA into two strands and each strand is surrounded by water that also forms spiky structures (Electronic Supporting Information Movie S1).

The evolution of the end-to-end distance of the dsDNA starting from a droplet of 6500 H_2O molecules is shown in Fig. 3. The $[dsDNA]^{20-}$ maintains its length in a droplet size of 6500–2000 H_2O molecules (panels (i) and (iii) in Fig. 2) even though the droplet is found in the charge-induced instability regime. The $[dsDNA]^{20-}$ extends and unwinds at the latest stage of solvent evaporation at droplet size of approximately 1500 H_2O molecules. The study of the unwinding of the dsDNA in the droplet shows that the droplet deformation precedes the change of the conformation of the dsDNA.

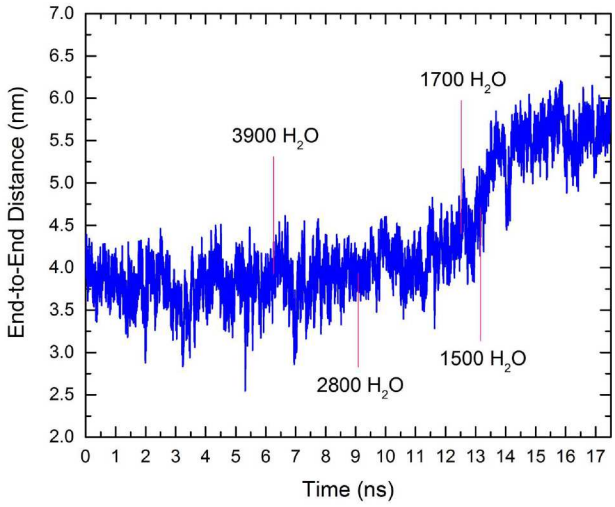

Fig. 3 End-to-end distance of dsDNA vs. time in the course of the droplet evaporation. The initial droplet was composed of 6500 water molecules. The evolution of the dsDNA end-to-end distance is that that corresponds to the droplet evaporation shown in Fig. 2. The length of a 11-base pair B-DNA that has been reported[43] is 3.74 nm, which is in agreement with the initial length of the dsDNA in the droplet of 6500 water molecules. At 12 ns, the droplet contained approximately 1800 H_2O molecules and at this point the unwinding of the dsDNA started to be noticeable. This conformation of the dsDNA corresponds in Fig. 2-iv. At 17 ns the end-to-end distance corresponds to the snapshot in Fig. 2-v.

The overall picture that arises from the simulations is that the droplet evolution during the desolvation of the DNA has several distinct features: The first prominent feature is the change in the droplet morphology from spherical, when the system is below the Rayleigh limit, to spiky when the system is above the Rayleigh limit. The origin of the dramatic shape change is addressed in the Sec. 3.1.1. The second feature is that the spiky morphology increases the surface area of the droplet and this in turn affects the evaporation mechanism. This feature is discussed in the Sec. 3.1.2. The third feature is that in the spiky droplets there is a high degree of solvent ordering because of the strong electric field of the complex.[33] This ordering can be realised by visual inspection. In this new environment the solvation of the dsDNA, or in general, of any other biological molecule is dramatically different from that in the bulk solution. Depending on the evaporation rate, the highly ordered droplet environment may affect the conformation of a macromolecule, the stability of a complex of macromolecules, or their charge state differently from that of the bulk solution. This third feature is not discussed in this manuscript in relation to the stability of dsDNA. In view of the variety of systems that are found in a droplet environment in ESI, this feature deserves a separate study.

Our studies on the stability of the $[dsDNA]^{20-}$ in pristine aqueous

droplets demonstrated that the $[dsDNA]^{20-}$ may be stable within the instability regime in the larger droplets. As long as there is sufficient amount of solvent to accommodate the instability the association of the macromolecules and their conformation may stay intact. The charge-induced instability is accommodated by the spiky formation of the solvent in the larger droplets, and it is only in the last stage of the droplet life-time that the dsDNA unwinds and separates into the two strands. The stability of dsDNA in the larger droplets might be realistic but we cannot also exclude the possibility that it may be force-field dependent. Therefore, one should view this finding as a proof of concept rather than as an exact result. The key point is that regardless of the true origin of the $[dsDNA]^{20-}$ stability in large droplets, we demonstrated that it is possible to have a charged macromolecule or a complex of macromolecules in a highly charged droplet without conformational changes.

At this point a discussion is in order about the relation of the simulations to experiments. DNA in deionised distilled water is expected to be denatured because of the low ionic strength of the solution.[44–49] The low ionic strength reduces the screening of the negative charges on the phosphate groups and leads to the dissociation of the dsDNA. In ESI-MS experiments $[CH_3COO]^-[NH_4]^+$ is often used in the bulk solution that contains the dsDNA. If a nanospray operates in the negative ion mode the initial droplets are expected to have excess negative charge. The negative charge stems from the negatively charged dsDNA, and CH_3COO^- ions. For instance, an initial droplet of 150 nm radius (which is the typical droplet size in nanospray) is expected to be composed by approximately a half billion water molecules, and 7320 e. For a concentration of $\approx 1 \times 10^{-4}$ M (used in the experiments of Light-Wahl et al.[28]) of single-stranded oligonucleotides in the bulk solution, it is expected that the initial droplet will contain of the order of 1000 single-stranded oligonucleotides. Thus, a substantial amount of the negative charge will be carried by the DNA strands. It is also expected that the droplets will contain a small number of NH_4^+ or Na^+ counterions. From the concentration of the bulk solution one infers that the majority of the smaller droplets with radius of a few nanometers will carry a single strand and possibly several droplets may hold at most two strands of DNA. Were the simulations started from two separate strands of DNA in a droplet it is expected the droplet to separate into two sub-droplets each carrying a DNA strand. Even if the droplet "cage" forces the association of the strands, the duplex will separate at the latest stage of the desolvation. It is also likely that some droplets will carry a DNA duplex. We showed that the duplex will also dissociate. These findings are in agreement with the ESI-MS experiments of Light-Wahl et al., who detected only the single strands by electrospraying dsDNA in distilled deionised water.[28] Regarding the mechanism of desolvation, spiky droplet morphologies will also appear during the desolvation of the single strands. The distinct features of the droplets with respect to its electrostatics, the evaporation rate, and the reactivity within the droplet will also be present for the single strands. These features will be maintained regardless of the length of the DNA.

3.1.1 Electrostatics of dsDNA

Analysis of the electrostatics in a droplet was used to understand the formation of spikes in the dsDNA-H_2O droplet. Comparison between Fig. 2 (i) and (ii) shows that when the droplet is in the charge-induced instability regime, the amount of H_2O around the backbone of the dsDNA decreases, but it increases near the termini of the duplex. Clearly, an amount of water migrates from the region near the backbone to the termini of the DNA duplex. During the droplet deformation from the spherical shape, the dsDNA unwinds into a rod-like shape as shown in Fig. 4a. We can visualise this conformation of the DNA duplex as a finite length charged-rod. Thus, we calculated the electrostatics of the dsDNA, using the Adaptive Poisson-Boltzmann Solver (APBS) software.[50] In Fig. 4a, a snapshot of $[dsDNA]^{20-}$ surrounded by $\sim$ 1700 H_2O molecules is shown with the electric field lines generated by the $[dsDNA]^{20-}$ alone. By far, the strongest electric field lines are close to the middle of the dsDNA backbone and the weakest are near the termini. This electric field pattern is typical of a finite length charge rod (Fig. 4c). Contrary to the intuitive expectation that the number of H_2O molecules will be higher in the regions of the strong electric field, we find that the H_2O molecules accumulate at the termini. The formation of the spikes at the dsDNA pole indicates that the droplet attains morphologies that disperse the charge as far as possible from the charged backbone. The spikes is a cooperative effect that cannot be predicted by the location of a few water molecules around the dsDNA.

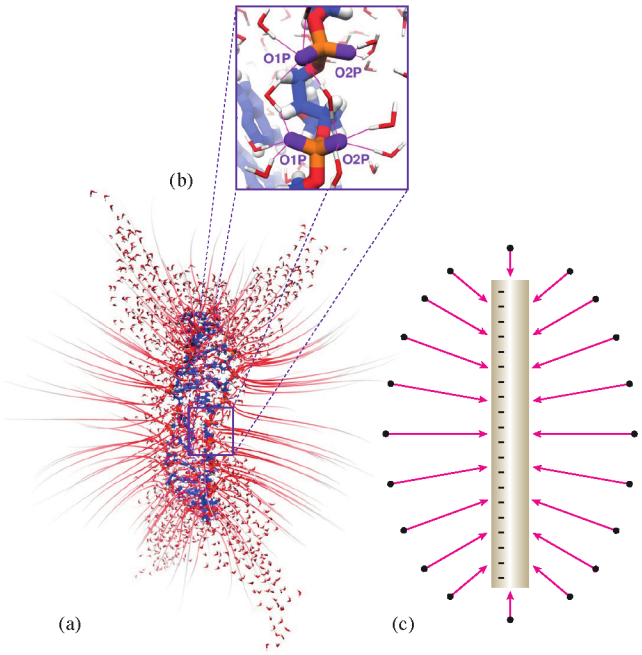

Fig. 4 (a) Solvated $[dsDNA]^{20-}$ in the instability regime with the electric field lines calculated for the bare $[dsDNA]^{20-}$. The intensity of the colour indicates the strength of the electric field. The field is stronger (red lines) near the middle of the backbone than that near the termini of the $[dsDNA]^{20-}$ where the intensity of the line colour decreases rapidly. In the region of $[dsDNA]^{20-}$ where the electric field is the strongest (middle region), the number of water molecules is smaller. (b) Inset for a zoomed-in region in (a) shows the H-bonds (pink lines) between the water and the oxygen atoms of the phosphate groups O1P and O2P (purple end-caps). (c) Schematic picture of the electric field surrounding a finite, negatively charged rod.

A possible explanation for the formation of the spikes at the termini is the following: Because of the fast diminishing electric potential near the termini of the duplex, the H_2O molecules have more freedom to build stronger H-bonds among them. In contrast, near the centre of the backbone where the electric potential is the strongest, the dipole moment of the H_2O molecules there are strongly aligned with the electric field. The strong alignment places a restriction on the H_2O freedom to build a strong H-bond network near the backbone. As a result, the H_2O molecules in the outer water-shells near the backbone migrate to the termini of the duplex where they construct large surfaces in the form of spikes.

Even though the most of the H_2O molecules are accumulated in the termini further into the instability regime, a shell of H_2O still surrounds the middle region of dsDNA as shown in Fig. 4a. The H_2O molecules in the first coordination shell of dsDNA form H-bonds with the O1P and O2P atoms on the backbone (Fig. 4b). The analysis of the H-bonding between the first-shell H_2O molecules and the oxygen atoms on the dsDNA backbone did not reveal any significant difference between the number of donated H-bonds in different charge states of nanodrops. The average number of H-bonds per O_1P or O_2P atoms, HOH···OP, is 2.8 in the aqueous nanodroplets that comprise $[dsDNA]^{20-}$, $[dsDNA]^{20-}$ and 10 Na^+ ions, $[dsDNA]^{20-}$ and 15 Na^+ ions. Thus, it appears that the H-bonding between the first-shell H_2O and the backbone is independent of the dsDNA conformation, uncoiled or coiled.

3.1.2 Solvent evaporation

The evaporation of water is a central process in the desolvation studies. We compare the evaporation rate of the charged droplet with that of a water droplet that contains a dsDNA with charge $-20\ e$ and 10 Na^+ (overall charge of the droplet $-10\ e$). In all the simulations, the initial droplet was composed of 6500 water molecules and the temperature was maintained at 350 K. The comparison of the evaporation rates of the two systems is shown in Fig. 5. We calculated the rate of water evaporation in the linear regime from 0 –10 ns for both nanodrops.

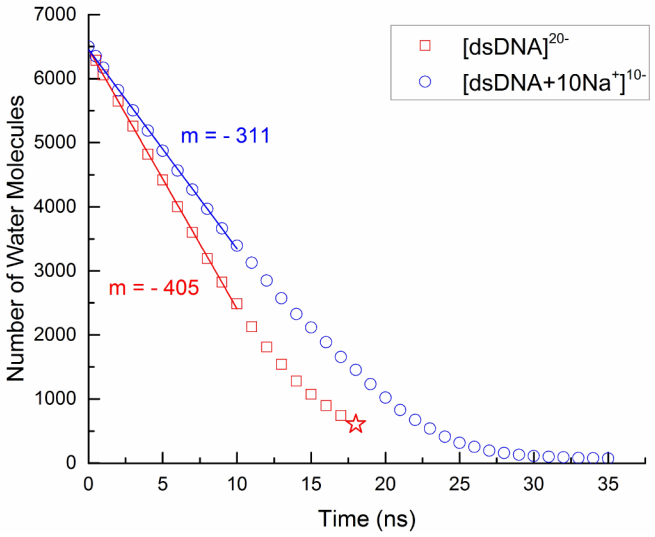

Fig. 5 Evaporation rate of water during the desolvation of dsDNA. The plot shows the number of water molecules remaining in the nanodrop for a given time. Linear fitting (from 0 to 10 ns) at T = 350 K shows that the desolvation rate of the nanodrop with larger net negative charge (red squares) equals to -405 H_2O molecules per ns; whereas, the desolvation rate of the nanodrop with smaller net negative charge (blue circles) is -311 H_2O molecules per ns. Denaturation of the DNA duplex in the highly charged nanodrop is indicated by a star at 17.5 ns.

We found that the evaporation rate of water molecules in the $[dsDNA]^{20-}$ nanodrop is 25% faster than the evaporation rate of water from the $[dsDNA + 10\,Na^+]^{10-}$ nanodrop. The faster rate of evaporation and the formation of spikes in a highly charged nanodrop are likely to be related. Because of the increased surface area created by the spikes, there is a relatively large number of water molecules located on the surface, which are more likely to evaporate. The linearity has been described by experimental studies on water drops placed on a solid surface.[51,52] Our results are consistent with those studies but merely during the initial desolvation of the dsDNA. We explain the initial linearity of the rate of water evaporation in the nanodrops that comprise the dsDNA by the different interactions among the water molecules in the coordination shells of the dsDNA. The H_2O molecules found in the outer-shells (far from the dsDNA) have weaker interactions with the dsDNA because of the screening effect of the inner-shell H_2O molecules and the separation distance from the dsDNA. Thus, the H_2O molecules in the outer-shells resemble those in a pure drop: their rate of evaporation is constant. In contrast, the inner-shell H_2O molecules have a relatively strong interaction with the dsDNA which dampens their rate of evaporation. The slowing-down of the evaporation starts earlier in the droplet of charge $-20\ e$ than the droplet with charge $-10\ e$.

3.2 Effect of ions on the desolvation of $[dsDNA]^{20-}$ from aqueous nanodrops

$[dsDNA + xNa^+ + xCl^-]^{20-}$ (x = 5, 10) in a 1500-H_2O droplet. In a set of simulations, we examined the effect of an initial equal concentration of Na^+ and Cl^- ions in the desolvation of dsDNA. In particular we studied $[dsDNA + xNa^+ + xCl^-]^{20-}$ (x = 5, 10) in droplets of 1500 H_2O molecules. These droplets were prepared in the charge-induced instability regime. The systems with x = 5 and 10 behave similarly during the desolvation process. We find that at the early stage of droplet evaporation Cl^- ions are released sequentially from the droplet. At the late stage of the desolvation process the dsDNA is surrounded by water molecules that formed spikes. The Na^+ ions remained in the droplet in the latest desolvation stage, they were bound to the dsDNA. In the systems that contained 5 Na^+ ions the dsDNA denatured by separation of the two strands (Electronic Supporting Information Movie S2), while in the systems with 10 Na^+ ions the dsDNA remained bound with the two strands sliding against each other. A more thorough discussion of the sliding is presented in the Sec. 3.4. Because of the similarities in the two systems we present here only the desolvation of $[dsDNA + 5\,Na^+ + 5\,Cl^-]^{20-}$ (Fig. 6(a)). Figure S1 in the Electronic Supporting Information illustrates the conformations of the desolvated $[dsDNA]^{-20}$ with the final charge states of -20, -15, -10, -8, and $-5\ e$.

In Fig. 6(a)-i the prominent feature is the formation of spikes because of the high charge. Differently from the spiky droplet morphologies that were shown in Fig. 2, the spikes in Fig. 6a-i are transient and emerge throughout the entire droplet. From those solvent extrusions the Cl^- ions are released (Electronic Supporting Information Movie S3). This relatively high instability is manifested by the ejection of Cl^- ions from the nanodrop despite the presence of Na^+ ions. The release of the Cl^- ions is discussed in the Sec. 3.3.

Since the co-ions evaporate, the net charge of these nanodrops becomes less negative (Fig. 6a-ii). The extent of the stability gained by the loss of the co-ions depends on the remaining concentration of the counterions. For instance, the ejection of the five Cl^- ions from the $[dsDNA + 5\,Na^+ + 5\,Cl^-]^{20-}$ droplet reduces the net negative charge from $-20\ e$ to $-15\ e$. However, as a result of the relatively low concentration of the counterions, the duplex "unzips" (denatures) into two strands (Fig. 6a-ii,iii). Similarly, the 10 Na^+ ions in the $[dsDNA + 10\,Na^+ + 10\,Cl^-]^{20-}$ nanodrop remain non-covalently bound to the dsDNA after the ejection of the 10 Cl^- ions and a substantial solvent evaporation. The composition of the final desolvation product of the droplet and its charge state are presented in Table 2 for all the systems that have been examined in this article.

$[dsDNA + xNa^+ + yCl^-]^{15-}$ (x = 5, 10, 15 and y = 0, 5, 10) in 1500-H_2O droplets. These systems show increased stability over the nanodrops with the initial charge of $-20\ e$. Initially the droplet is found in the instability regime (Fig. 6b-i) as it is evidenced by the formation of spikes on the surface of the droplet. In Fig. 6b-i,ii, there is a clear trend of decreasing number and length of the spikes. Since the droplets with charge $-12\ e$ are close to the stability regime not all of the Cl^- ions are released readily from the aqueous droplet of dsDNA (Fig. 7). We find that that the release of Cl^- ions ceases when the net charge of the nanodrop, of any volume, is less negative than $-10\ e$, which is 50% of the dsDNA charge. This rather intriguing finding might be due to the relatively high concentration of Na^+ ions in these nanodrop. For example, seven Cl^- are ejected from the $[dsDNA + 15\,Na^+ + 10\,Cl^-]^{15-}$ nanodrop; its final state in the gas phase is $[dsDNA + 15\,Na^+ + 3\,Cl^-]^{8-}$. Whereas, all of the Cl^- ions in $[dsDNA + 10\,Na^+ + 5\,Cl^-]^{15-}$ are ejected from the nanodrop; its final state in the gas phase is $[dsDNA + 10\,Na^+]^{10-}$. In the latest stage of desolvation, in all cases of the set of runs with droplet charge $-15\ e$, the dsDNA maintains the double-stranded state in the gas phase and it is surrounded by Na^+ ions (Table 2).

$[dsDNA + xNa^+ + yCl^-]^{10-}$ (x = 10, 15, 20 and y = 0, 5, 10) and $[dsDNA + xNa^+ + yCl^-]^{10-}$ (x = 15, 20, 25 and y = 0, 5, 10) in 1500-H_2O droplets. The effect of the net charge on a nanodrop stability is more pronounced in the -10 and $-5\ e$ nanodrops. Comparison of the snapshots in Fig. 6c,d with those in Fig. 6a,b shows that the nanodrops with smaller net charge have smoother surfaces than the nanodrops with larger net charge. In the $-10\ e$ and $-5\ e$ nanodrops, the majority of the Cl^- ions are not ejected. The consequence of this is the dissolution of NaCl aggregates (Fig. 6c–ii, iii,d –ii, iii).

The dissolution of salt in the nanodrops increases during the desolva-

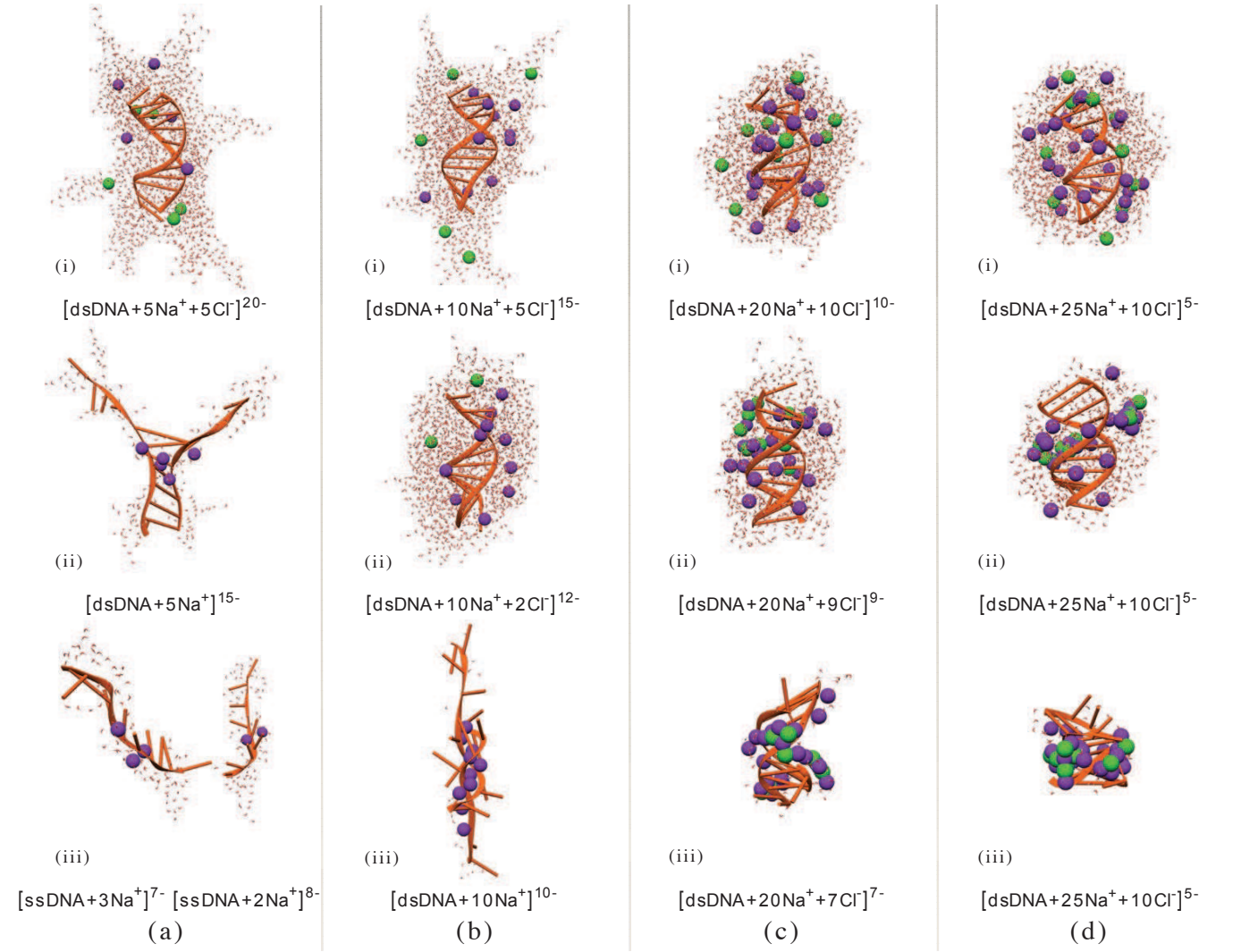

Fig. 6 Desolvation of dsDNA from a droplet that contains 1500 H_2O molecules, Na^+ and Cl^- ions. The initial nanodroplet carries a negative charge that may change during desolvation. The snapshots in each column show (i) the initial state of the droplet, (ii) an intermediate state, and (iii) the dsDNA at the latest stage of the desolvation, where it is almost bare of water molecules.

tion process. It is apparent from the desolvation snapshots in Fig. 6c, d that the salt dissolution increases gradually in the nanodrop, for the nanodrop size decreases throughout the desolvation of the dsDNA. We observe "transient" aggregations of NaCl. Some of these aggregations are in the form of $[2\,Na^+ + Cl^-]$ in the nanodrops that comprised ~ 600 H_2O(Fig. 6c-ii,d-ii); then, permanent dissolution of NaCl in the smaller nanodrops (Fig. 6c-iii,d-iii). Similar aggregation has been found in our previous study on the effect of counterions on the charging of a macromolecule.[42] In particular, we have found that the $[Cl^- - 2Na^+]$ complexes are formed in large droplets where the concentration of Na^+ and Cl^- ions are low. Then, larger aggregates were increasingly formed, as the concentration of the ions increased. The increase in ion concentration was a result of the continued decrease in droplet volume.

3.3 How does a charged droplet accommodate the instability?

In the Sec. 3.1 and 3.2 we demonstrated that the charge of the droplet in the instability regime is dispersed via three mechanisms: (i) by release of charged species when the charged species found in the droplets are non-covalently bound to macromolecules; (ii) by spiky formations of the solvent distribution when the charged species are covalently bound to macromolecules; and (iii) by unwinding of the dsDNA when the solvent surface is not sufficient to disperse the charge away from the charged macromolecule. In our studies, examples of (i) are the release of the Cl^- ions from droplets containing dsDNA and the separation of the two strands of dsDNA when they are found at certain charge states at the latest stage of a droplet lifetime. Manifestation of (ii) is the formation of spikes on the surface of the droplet that increase its surface area. The third mechanism is demonstrated by the unwinding of the dsDNA at the later stage of the droplet lifetime. We have found instances where mechanisms (i) and (ii) may take effect concurrently. In this event, the presence of the spikes may affect the manner that a single ion is released relative to systems where all the charges are not bound to each other. In this section we discuss these mechanisms across the spectrum of all the dsDNA systems that have been studied for this manuscript.

Fragmentation of the droplet. Fig. 7 shows the net charge of 1500 H_2O nanodrops during desolvation. For comparison, the estimated Rayleigh prediction is also shown. The estimated Rayleigh limit for the 1500 H_2O nanodrop at $T = 350$ K is $-10\ e$. In the Rayleigh estimate, we used an approximate surface tension value of 0.0432 Nm^{-1} for TIP3P water model at $T = 350$ K[41]. The initial droplet states with charge $-20\ e$ and $-15\ e$ are above the Rayleigh limit. In these droplets Cl^- ions are readily released so as the droplet charge is lowered near to that predicted

by the Rayleigh limit. Fig. 7 shows that droplets with initial charge of $-10\ e$ may sustain charge above the Rayleigh limit. This is attributed to the formation of salt aggregates that prevent the release of Cl^- ions as was discussed in the Sec. 3.2.

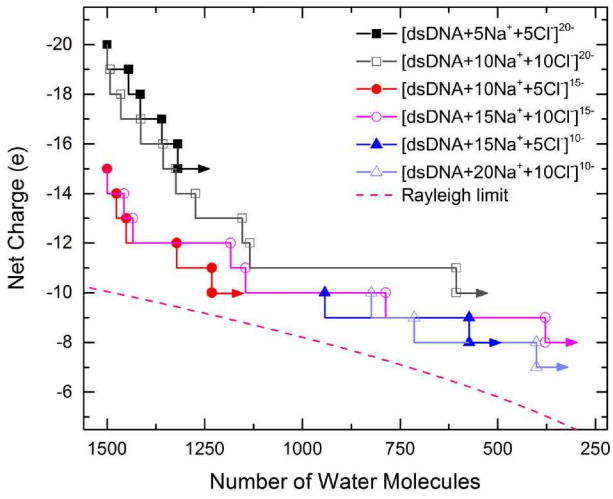

Fig. 7 The net charge of a water nanodrop in its journey to the gas phase vs. the number of H_2O molecules. The legends indicate the initial composition and the charge of each nanodrop. Each symbol indicates the net charge of the nanodrop prior to a single Cl^- ion evaporation. The change in the charge is illustrated by a vertical line from the data point followed by a horizontal line that indicates the water evaporation before reaching a new critical charge. The Rayleigh limit (– – –) was calculated using the surface tension value of $\gamma = 0.0432\ \mathrm{Nm}^{-1}$ [41] at T = 350 K. The last net charge (indicated by an arrow) did not change throughout the transition to the gas phase.

This existence of droplets above the Rayleigh limit is to be contrasted with that of our previous study on positively charged aqueous nanodrops that contained a poly(ethylene glycol) and Na^+ ions.[42] In those droplets, the net charge of the droplet was sustained slightly below the Rayleigh limit because of the interactions of the poly(ethylene glycol) with the Na^+ ions.

Increase of the surface area to volume ratio. To assess the correlation between the charge-induced instability and the surface area of the nanodrops that comprise the DNA duplex, we analysed the surface-area-to-volume ratio (SA:V) of these nanodrops. Fig. 8 shows the average SA:V of each of the four sets of droplet charge states that we studied. The SA:V values were calculated for a nanodrop at a volume of 59 nm^3. The average SA:V ratio of six observations in the $-5\ e$ nanodrops set was approximately 4% smaller than that of the -10 e, 17% smaller than that of the $-15\ e$ and 29% smaller than that of the $-20\ e$ nanodrops. The analysis shows that in general nanodrops with relatively small net charge have a smaller SA:V.

These results confirm the relation between the charge-induced instability and the shape of a charged nanodrop. This relation may partly be explained by comparing the SA:V ratio of the charged nanodrops with the SA:V of simple geometrical shapes. Among all of the shapes, the sphere has the smallest SA:V. Whereas, the spike shape has, by far, larger SA:V than that of a smooth sphere. The shapes of the nanodrops that we studied ranged from a sphere ($-5\ e$) to a star polygon ($-20\ e$). This variation in geometry reflects the instability of the charged droplet. A stable nanodrop has a smaller SA:V than that of an unstable nanodrop.

We also examined the number of H-bonds between H_2O molecules, which are shown in Fig. 9. The average number of $H_2O\cdots H_2O$ H-bonds per H_2O of six observations in the $-5\ e$ nanodrops is 5.4% larger than that in the $-20\ e$ nanodrops (Fig. 9). We found a small effect of the presence of Cl^- ions in the number of H-bonds between H_2O molecules. We can say that the number of H-bonds between the water in nanodrops, in general,

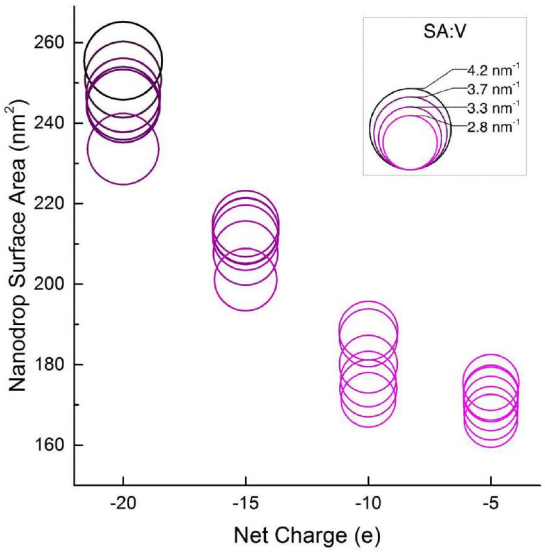

Fig. 8 Average surface area and surface-to-volume ratio (SA:V) of aqueous nanodrops with various charges. The surface area values for nanodrops of an equal volume, which is 59 nm^3 are plotted against the net charge of the correspondent nanodrop. The position of the bubble on the graph indicates the nanodrop surface area whereas the size indicates its SA:V ratio. The darker and larger bubbles indicate a relatively large SA:V.

appear to be dependent on the net charge.

Our findings on the number of H-bonds between H_2O molecules mirror those of the relation between the charge-induced instability and the surface area of a nanodrop. The overall trend in Fig. 9 indicates that the H_2O molecules in a relatively unstable nanodrop form fewer intermolecular H-bonds than in a more stable one. This trend can be attributed to the larger number of H_2O molecules on the relatively large surface of an unstable nanodrop. These H_2O molecules form fewer hydrogen bonds because they are found on the surface.

Cation interactions and the unwinding of the DNA duplex. The charge-induced instability of the nanodrop that comprises the dsDNA is also expressed by the unwinding of the DNA duplex. This can be explained by the relatively low concentration of cation with respect to that of the anion. To assess how the DNA duplex unwinds in an unstable charged nanodrop, we first examine the duplex stability in a counterion-containing nanodrop. Figure 10 shows the minor groove width of the DNA duplex in a droplet composed of 6500 H_2O and 10 Na^+ ions. During the desolvation process, there is a clear trend of increase in the association strength between the Na^+ and the oxygen atoms of the dsDNA phosphodiester linkages across the two strands ($A{-}O_1P\cdots\ Na^+\cdots O_1P{-}T$). The increasing strength of this association can be explained by the reduction of the $Na^+\cdots\ O_1P$ distance fluctuations. This strong association between a Na^+ and the backbone of dsDNA is consistent with the X-ray findings that monovalent cations are strongly associated with nucleic acids at the minor groove.[53] The interesting point in our data is the decreasing width of the dsDNA minor groove. The $O_1P\cdots O_1P$ distance across the A·T strands (A-O1P...O1P-T) decreases from 8.3 in the droplet to 2.9 in the gas phase (Fig. 10). Over the initial 10 ns of the dsDNA desolvation, the mean separation distance of 8.3 agrees well with the X-ray data of A·T-rich dsDNA.[54–56] A possible explanation to the narrowing of the minor groove is that the cation association with the backbone shields the repulsion between the negative charges on the two strands. This can be viewed as a three-site interaction between a Na^+ and two of the phosphodiester oxygen atoms located across the two strands: $(O_1P)^{0.5-}\cdots\ (Na)^{1+}\cdots\ (O_1P)^{0.5-}$ (inset in Fig. 10). Collectively, Na^+ brings the two strands of the dsDNA closer; thus, Na^+ narrows the minor

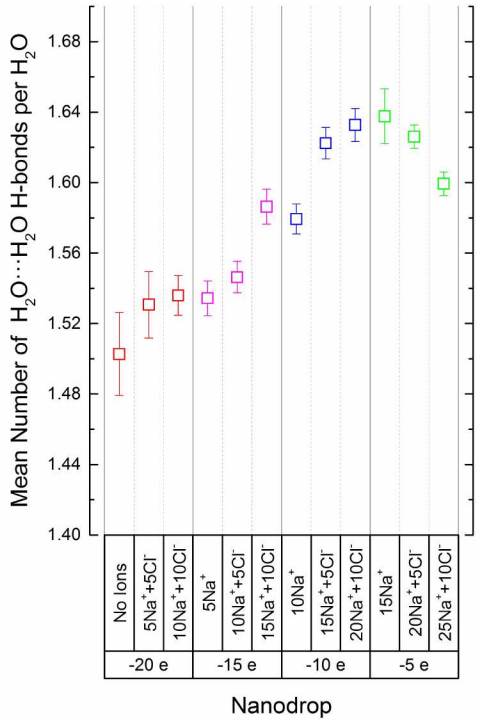

Fig. 9 Average number of H-bonds per water molecule for droplets of various charge states. The average numbers of H-bonds per water molecule of each initial condition was calculated for nanodrops composed of 1500 H_2O molecules, a $[dsDNA]^{20-}$, and ions (horizontal table).

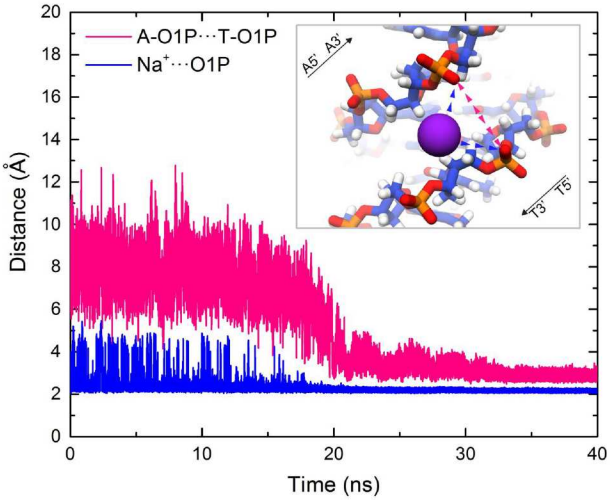

Fig. 10 Distance of an Na^+ from the minor groove of dsDNA during droplet desolvation. As the dsDNA desolvates, the Na^+ ions move towards the minor groove and the separation between the two strands decreases. The strength of Na^+ association into the minor groove increases as indicated by the decrease in the distance fluctuations of $Na^+\cdots O_1P$ interactions. For clarity, we merely show $Na^+\cdots O_1P$ but similar trend was observed in $Na^+\cdots O_2P$ distance. The inset shows the unfavourable interaction between the O1P atoms (opposing arrow heads) and the favourable interaction that attracts the Na^+ ions towards the minor groove.

groove.

In contrast, the DNA duplex unwinds in a highly negative charged droplet. As we discussed in Fig. 3, the end-to-end distance of the dsDNA increases in the droplet that contains no counterions. Similarly, the dsDNA unwinds and denatures in highly charged droplets. These droplets contain either a low $[Na^+]$ or a small $[Na^+]/[Cl^-]$. The observed decrease of the minor groove width in droplets with relatively small negative charge and the unwinding of the DNA duplex in droplets with large negative charge suggests that the small $[Na^+]/[Cl^-]$ ratio is the main factor in the unwinding of the DNA duplex. Thus, in a droplet with highly negative charge the dsDNA unwinds to reduce the repulsion between the negative charges of the phosphate groups across the DNA strands.

3.4 Characterisation of the DNA structure in the gas phase

In the previous discussion, we characterised the instability of nanodrops that contained $[dsDNA]^{20-}$ and analysed the manifestation of charge-induced instability during the desolvation process. We will now turn to discuss the final stage in the dsDNA desolvation: DNA in the gas phase.

Minimum charge to maintain a duplex. The first question in this study sought to determine the stability of DNA duplex the in gas phase; will it denature? The final ion composition in nanodrops and the net charge on the DNA are shown in Table 2. Three important observations emerge from the data in Table 2. First, the dsDNA denatures in nanodrops that have less than 10 Na^+ ions, in other words, where the cation charge is less than half the absolute value of the dsDNA charge. Second, the ejection of Cl^- ions ceases when the net charge was less negative than $-10\ e$. Third, in all cases none of Na^+ ions is evaporated.

It is apparent from the data in Table 2 that the dsDNA charge state, after desolvation, is the major contributing factor to its stability in the gas phase. For example, the double-stranded state is maintained when the final charge is less negative than $-10\ e$. The preceding discussion on the fragmentation of the droplet showed that Cl^- ions were ejected to stabilise the nanodrop. Because all the nanodrops that we studied had a net negative charge, none of the Na^+ ions evaporated. Based on these two findings, the ejection of Cl^- ions and the holding of the Na^+ ions, we can predict the final charge state and thus the stability of the DNA duplex in the gas phase.

Conformations of DNA in the gas phase. We identified three tertiary structures of the dsDNA in the gas phase: denatured, double-stranded, and inverted zipped-up DNA. As discussed above, the dsDNA denatured when the final negative charge it carried was above 50% of the fully deprotonated dsDNA charge (Fig. 6a-iii). In contrast, when the final negative charge was below 50% of the isolated dsDNA charge, the dsDNA maintained a duplex state. As shown in Fig. 6c-iii,d-iii there is a clear difference in the degree of duplex compactness. The less negative dsDNA in Fig. 6d-iii ($-5\ e$) is more compact than the dsDNA in Fig. 6c-iii ($-10\ e$).

The most intriguing conformation that we identified for the dsDNA in the gas phase is the "inverted zipped-up" (Fig. 6b-iii). We found this conformation in the all desolvated dsDNA that carried a net charge of $-10\ e$. Data from electrospray experiments[57–59] suggested that the two strands remained bound in the gas phase. However, very little was found in the literature on the question of the negative charge limit to maintain the DNA duplex in the gas phase. Gabelica et al. data[59] on a 12-mer dsDNA suggested that the duplex state is maintained for a net charge that was less negative than -5 e, ~25% of the fully deprotonated 12-mer dsDNA charge. Because of the complexity of real systems we cannot argue that our computational study replicates the experiment. However, our findings generally agree with those obtained in electrospray that the dsDNA can maintain it double-stranded state if its net charge in the gas phase is less than half its isolated charge.

The 50% net charge DNA in the gas phase was an exceptional case. During the transition from nanodrop to the gas phase, the duplex of $[dsDNA + 10\,Na^+]^{10-}$ zipped-up. The zipping-up formed partially bound strands in the centre and two unbound halves at the terminals; creating a "knot". The illustration in Fig. 11 shows that Na^+ ions concentrate at the knot where they form adducts with the the backbone of DNA; as a result, Na^+ ions created a neutral region. The unbound halves of the two

Table 2 State of the 11-mer dsDNA-residue and charge in the gas phase. The dashes denote the aqueous droplets with no ions. These droplets contain only a dsDNA and no ions. The initial nanodrop composition corresponds to that of Table I. It is noted that (i) dsDNA denatures into two strands in the gas phase when the net charge of the dsDNA-residue is more negative than $-10\ e$; and (ii) there is no Cl^- ion evaporation when the net negative charge is equal to or less than $-5\ e$.

Initial ion composition		Gas phase		
Ions	Net charge/e	Remaining ions	DNA-residue charge/e	DNA state
-[a]	-20	-	-20	denatured
-	-20	-	-20	denatured
$5\,Na^+ + 5\,Cl^-$	-20	$5\,Na^+$	-15	denatured
$5\,Na^+$	-15	$5\,Na^+$	-15	denatured
$10\,Na^+ + 10\,Cl^-$	-20	$10\,Na^+$	-10	inverted zipped-up[b]
$10\,Na^+ + 5\,Cl^-$	-15	$10\,Na^+$	-10	inverted zipped-up[b]
$10\,Na^+$[a]	-10	$10\,Na^+$	-10	inverted zipped-up[b]
$10\,Na^+$	-10	$10\,Na^+$	-10	inverted zipped-up[b]
$15\,Na^+ + 10\,Cl^-$	-15	$15\,Na^+ + 3\,Cl^-$	-8	duplex
$15\,Na^+ + 5\,Cl^-$	-10	$15\,Na^+ + 3\,Cl^-$	-8	duplex
$20\,Na^+ + 10\,Cl^-$	-10	$20\,Na^+ + 7\,Cl^-$	-7	duplex
$15\,Na^+$	-5	$15\,Na^+$	-5	duplex
$20\,Na^+ + 5\,Cl^-$	-5	$20\,Na^+ + 5\,Cl^-$	-5	duplex
$25\,Na^+ + 10\,Cl^-$	-5	$25\,Na^+ + 10\,Cl^-$	-5	duplex

[a] Initial droplet comprised 6500 water molecules. [b] Illustration for the inverted zipped-up structure is shown in Fig. 11.

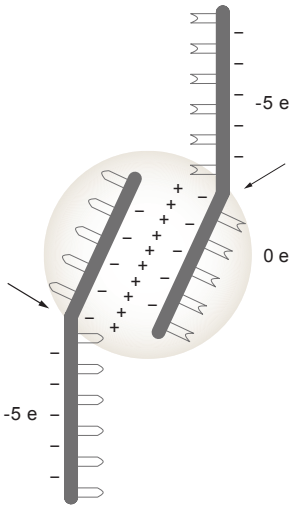

Fig. 11 Schematic picture of the $[\text{dsDNA} + 10\,Na^+]^{10-}$ conformation and charge distribution in gas phase. During the transition of $[\text{dsDNA} + 10\,Na^+]^{10-}$ from the droplet into the gas phase, the two strands slid in opposite direction about half their length. The two strands twist at the points indicated by two arrows such that their backbones are held together by the excess of Na^+ ions. There is no net charge in the central region (highlighted by the bubble), where the two halves of the strands are held together by 10 Na^+ ions. The exposed halves contribute a net charge of $-10\ e$.

strands contributed a net charge of $-10\ e$. The location of the Na^+ ions in the centre of DNA and the location of the negative charge of DNA at the termini agrees with the experimental findings of Favre et al.[60,61] It is important to note that this is not a zipping-up of the DNA duplex; the two strands twisted so that their bases in the knot region pointed outward. The overall mechanism can be thought of as an "inverted" zipping-up of the DNA duplex.

4 Conclusions

We presented the desolvation mechanism of a double-stranded oligodeoxynucleotide (dsDNA) from a charged aqueous droplet. The dsDNA carried its full negative charge and it was embedded in two droplet environments: (i) pristine aqueous droplets and (ii) droplets that contained Na^+ and Cl^- ions at various concentrations. A common mechanism of desolvation in all the droplets of various ion concentrations was solvent evaporation. The desolvation also proceeded by the release of solvated Cl^- ions in droplets with Na^+ and Cl^- ions. During the desolvation, we studied the role of two key effects into the stability of dsDNA: the distinct droplet morphologies that arise from the charge-induced instabilities and the increase in the ion concentration during the shrinking of the droplet. We find that aqueous droplets that contain $[\text{dsDNA}]^{n-}$ $(n = 20)$ with and without Na^+ ions may attain spiky morphologies when the overall charge of the droplet is above the Rayleigh limit. The formation of spiky structures on the surface of the solvent is a way for the system to manifest the charge-induced instability when the charge is bound along the backbone of a macromolecule or complex of macromolecules. This form of instability is a general feature of the behaviour of charged droplets with bound charge that it is expected to hold regardless of the length of the dsDNA or even more so, of the nature of the macromolecule. One can envisage that charged aqueous droplets of dsDNA with a small number of counterions (for instance with the commonly used NH_4^+ or Na^+ ions) may be present in electrospray ionization (ESI) aerosols especially when distilled deionised aqueous solution is sprayed in the negative ion mode. We demonstrated the possibility that in the instability regime a complex may stay intact as long as there is sufficient amount of solvent to accommodate the instability by the formation of spikes. The complex may dissociate only in the last stage of the droplet life-time when there is not enough solvent to transfer away the polarisation charge from the complex.

In droplets with ions, Na^+ ions may form adducts with the double helical DNA in the minor groove. The adducts help to stabilise the duplex state in the gas phase. The negative ions may be released from the droplet, while no positive ions are released. In higher concentrations of Na^+ and Cl^- ions, at the latest stage of desolvation, sodium chloride aggregates are formed on the surface of dsDNA. In a DNA-droplet with a net charge that is less negative than 50% of the DNA charge, the DNA maintains the double-stranded state in the gas phase. However, the conformation of the dsDNA may change depending on the location of the ions on the strands. In ESI, it is common to have NH_4^+ counterions. Even though in the presented simulations we studied Na^+ ions, our findings can be generalised for the case of NH_4^+ ions. Several studies have examined the binding of NH_4^+ in DNA in the bulk solution.[62–64] All the studies agree that NH_4^+ ions may bind in the minor groove of dsDNA in a similar manner to Na^+ ions.

In summary, the presented study allowed us to identify general features pertinent to the desolvation process of complexes of macromolecules from droplets. Our findings may assist to determine ESI conditions in a systematic manner so as the association properties of complexes are preserved

between the bulk solution and the gas phase.

Acknowledgment

SC acknowledges the Discovery Grant of Natural Sciences and Engineering Research Council of Canada (NSERC) and a Marie Curie International Incoming Fellowship held at the Department of Chemistry, University of Cambridge, United Kingdom for funding this research. Compute Canada is acknowledged for providing the computing facilities. SC thanks Prof. Daan Frenkel, Department of Chemistry, University of Cambridge for his always insightful questions and comments.

References

1 A. J. Heck and R. H. van den Heuvel, *Mass Spectrom. Rev.*, 2004, **23**, 368–389.
2 F. Sobott and C. V. Robinson, *Curr. Opin. Struct. Biol.*, 2002, **12**, 729–734.
3 J. L. Benesch and C. V. Robinson, *Curr. Opin. Struct. Biol.*, 2006, **16**, 245–251.
4 G. R. Hilton and J. L. Benesch, *J. R. Soc. Interface*, 2012, rsif20110823.
5 J. A. Loo, *Mass Spectrom. Rev.*, 1997, **16**, 1–23.
6 S. H. Lomeli, S. Yin, R. R. Ogorzalek Loo and J. A. Loo, *J. Am. Soc. Mass Spectrom.*, 2009, **20**, 593–596.
7 E. N. Kitova, N. Soya and J. S. Klassen, *Anal. Chem.*, 2011, **83**, 5160–5167.
8 K. Barylyuk, R. M. Balabin, D. Grünstein, R. Kikkeri, V. Frankevich, P. H. Seeberger and R. Zenobi, *J. Am. Soc. Mass Spectrom.*, 2011, **22**, 1167–1177.
9 A. El-Hawiet, E. N. Kitova, L. Liu and J. S. Klassen, *J. Am. Soc. Mass Spectrom.*, 2010, **21**, 1893–1899.
10 Z. Hall, H. Hernández, J. A. Marsh, S. A. Teichmann and C. V. Robinson, *Structure*, 2013, **21**, 1325–1337.
11 J. a. Marsh, H. Hernández, Z. Hall, S. E. Ahnert, T. Perica, C. V. Robinson and S. a. Teichmann, *Cell*, 2013, **153**, 461–470.
12 J. A. Marsh, H. Hernández, Z. Hall, S. E. Ahnert, T. Perica, C. V. Robinson and S. A. Teichmann, *Biophys J*, 2013, **104**, 391a.
13 C. Schmidt and C. V. Robinson, *FEBS J.*, 2014, **281**, 1950–1964.
14 P. Kebarle and U. H. Verkerk, *Mass Spectrom. Rev.*, 2009, **28**, 898–917.
15 N. B. Cech and C. G. Enke, *Mass Spectrom. Rev.*, 2001, **20**, 362–387.
16 S. Consta, K. R. Mainer and W. Novak, *J. Chem. Phys.*, 2003, **119**, 10125–10132.
17 K. Ichiki and S. Consta, *J. Phys. Chem. B*, 2006, **110**, 19168–19175.
18 S. Consta and A. Malevanets, *Phys. Rev. Lett.*, 2012, **109**, 148301.
19 F. A. Sheriff and S. Consta, *Can. J. Chem.*, 2014, **93**, 1–8.
20 S. Consta, M. I. Oh and S. Soltani, *Int. J. Mass Spectrom.*, 2014, **377**, 557–567.
21 S. Consta and A. Malevanets, *Mol. Simul.*, 2015, **41**, 73–85.
22 T. L. Pukala, B. T. Ruotolo, M. Zhou, A. Politis, R. Stefanescu, J. A. Leary and C. V. Robinson, *Structure*, 2009, **17**, 1235–1243.
23 S. Consta and J. K. Chung, *J. Phys. Chem. B*, 2011, **115**, 10447–10455.
24 B. J. Conner, A. A. Reyes, C. Morin, K. Itakura, R. L. Teplitz and R. B. Wallace, *Proc. Natl. Acad. Sci.*, 1983, **80**, 278–282.
25 R. B. Wallace, M. J. Johnson, T. Hirose, T. Miyake, E. H. Kawashima and K. Itakura, *Nucleic Acids Res.*, 1981, **9**, 879–894.
26 S. V. Suggs, R. B. Wallace, T. Hirose, E. H. Kawashima and K. Itakura, *Proc. Natl. Acad. Sci.*, 1981, **78**, 6613–6617.
27 O. Boussif, F. Lezoualc'h, M. A. Zanta, M. D. Mergny, D. Scherman, B. Demeneix and J. P. Behr, *Proc. Natl. Acad. Sci.*, 1995, **92**, 7297–7301.
28 K. J. Light-Wahl, D. L. Springer, B. E. Winger, C. G. Edmonds, D. G. Camp, B. D. Thrall and R. D. Smith, *J. Am. Chem. Soc.*, 1993, **115**, 803–804.
29 D. L. Beveridge and K. J. McConnell, *Curr. Opin. Struct. Biol.*, 2000, **10**, 182–196.
30 A. D. MacKerell and N. K. Banavali, *J. Comput. Chem.*, 2000, **21**, 105–120.
31 T. E. Cheatham III, *Curr. Opin. Struct. Biol.*, 2004, **14**, 360–367.
32 M. Rueda, S. G. Kalko, F. J. Luque and M. Orozco, *J. Am. Chem. Soc.*, 2003, **125**, 8007–8014.
33 S. Consta, *J. Phys. Chem. B*, 2010, **114**, 5263–5268.
34 F. Lord Rayleigh, *Philos. Mag. Ser. 5*, 1882, **14**, 184–186.
35 B. A. Thomson and J. V. Iribarne, *J. Chem. Phys.*, 1979, **71**, 4451–4463.
36 J. V. Iribarne and B. a. Thomson, *J. Chem. Phys.*, 1976, **64**, 2287–2294.
37 W. L. Jorgensen, J. Chandrasekhar, J. D. Madura, R. W. Impey and M. L. Klein, *J. Chem. Phys.*, 1983, **79**, 926.
38 S. Pronk, S. Páll, R. Schulz, P. Larsson, P. Bjelkmar, R. Apostolov, M. R. Shirts, J. C. Smith, P. M. Kasson, D. van der Spoel, B. Hess and E. Lindahl, *Bioinformatics*, 2013, btt055.
39 W. Humphrey, A. Dalke and K. Schulten, *J. Mol. Graph.*, 1996, **14**, 33–38.
40 K. Lindorff-Larsen, S. Piana, K. Palmo, P. Maragakis, J. L. Klepeis, R. O. Dror and D. E. Shaw, *Proteins Struct. Funct. Bioinforma.*, 2010, **78**, 1950–1958.
41 C. Vega and E. de Miguel, *J. Chem. Phys.*, 2007, **126**, 154707.
42 M. Sharawy and S. Consta, *J. Chem. Phys.*, 2014, **141**, 104321.
43 R. Wing, H. Drew, T. Takano, C. Broka, S. Tanaka, K. Itakura and R. E. Dickerson, *Nature*, 1980, **287**, 755–758.
44 J. Marmur and P. Doty, *J. Mol. Biol.*, 1962, **5**, 109–118.
45 C. Schildkraut and S. Lifson, *Biopolymers*, 1965, **3**, 195–208.
46 J. G. Wetmur and J. Fresco, *Crit. Rev. Biochem. Mol. Biol.*, 1991, **26**, 227–259.
47 M. D. Frank-Kamenetskii, *Biopolymers*, 1971, **10**, 2623–2624.
48 R. D. Blake and S. G. Delcourt, *Nucleic Acids Res.*, 1998, **26**, 3323–3332.
49 R. Owczarzy, Y. You, B. G. Moreira, J. A. Manthey, L. Huang, M. A. Behlke and J. A. Walder, *Biochemistry (Mosc.)*, 2004, **43**, 3537–3554.
50 N. A. Baker, D. Sept, S. Joseph, M. J. Holst and J. A. McCammon, *Proc. Natl. Acad. Sci.*, 2001, **98**, 10037–10041.
51 K. S. Birdi, D. T. Vu and A. Winter, *J. Phys. Chem.*, 1989, **93**, 3702–3703.
52 M. Dandan and H. Y. Erbil, *Langmuir*, 2009, **25**, 8362–8367.
53 X. Shui, C. C. Sines, L. McFail-Isom, D. VanDerveer and L. D. Williams, *Biochemistry (Mosc.)*, 1998, **37**, 16877–16887.
54 F. J. Acosta-Reyes, C. Dardonville, H. P. de Koning, M. Natto, J. A. Subirana and J. L. Campos, *Acta Crystallogr. D Biol. Crystallogr.*, 2014, **70**, 1614–1621.
55 F. J. Acosta-Reyes, J. A. Subirana, J. Pous, R. Sánchez-Giraldo, N. Condom, R. Baldini, L. Malinina and J. L. Campos, *Biopolymers*, 2015, **103**, 123–133.
56 J. Aymami, C. M. Nunn and S. Neidle, *Nucleic Acids Res.*, 1999, **27**, 2691–2698.
57 D. C. Gale and R. D. Smith, *J. Am. Soc. Mass Spectrom.*, 1995, **6**, 1154–1164.
58 S. A. Hofstadler and R. H. Griffey, *Chem. Rev.*, 2001, **101**, 377–390.
59 V. Gabelica, E. De Pauw and F. Rosu, *J. Mass Spectrom.*, 1999, **34**, 1328–1337.
60 A. Favre, F. Gonnet and J.-C. Tabet, *Int. J. Mass Spectrom.*, 1999, **190–191**, 303–312.
61 A. Favre, F. Gonnet and J.-C. Tabet, *Eur. J. Mass Spectrom.*, 2000, **6**, 389.
62 N. V. Hud, V. Sklenář and J. Feigon, *J. Mol. Biol.*, 1999, **286**, 651–660.
63 M. A. Young, B. Jayaram and D. L. Beveridge, *J. Am. Chem. Soc.*, 1997, **119**, 59–69.
64 K. Phillips, Z. Dauter, A. I. H. Murchie, D. M. J. Lilley and B. Luisi, *J. Mol. Biol.*, 1997, **273**, 171–182.